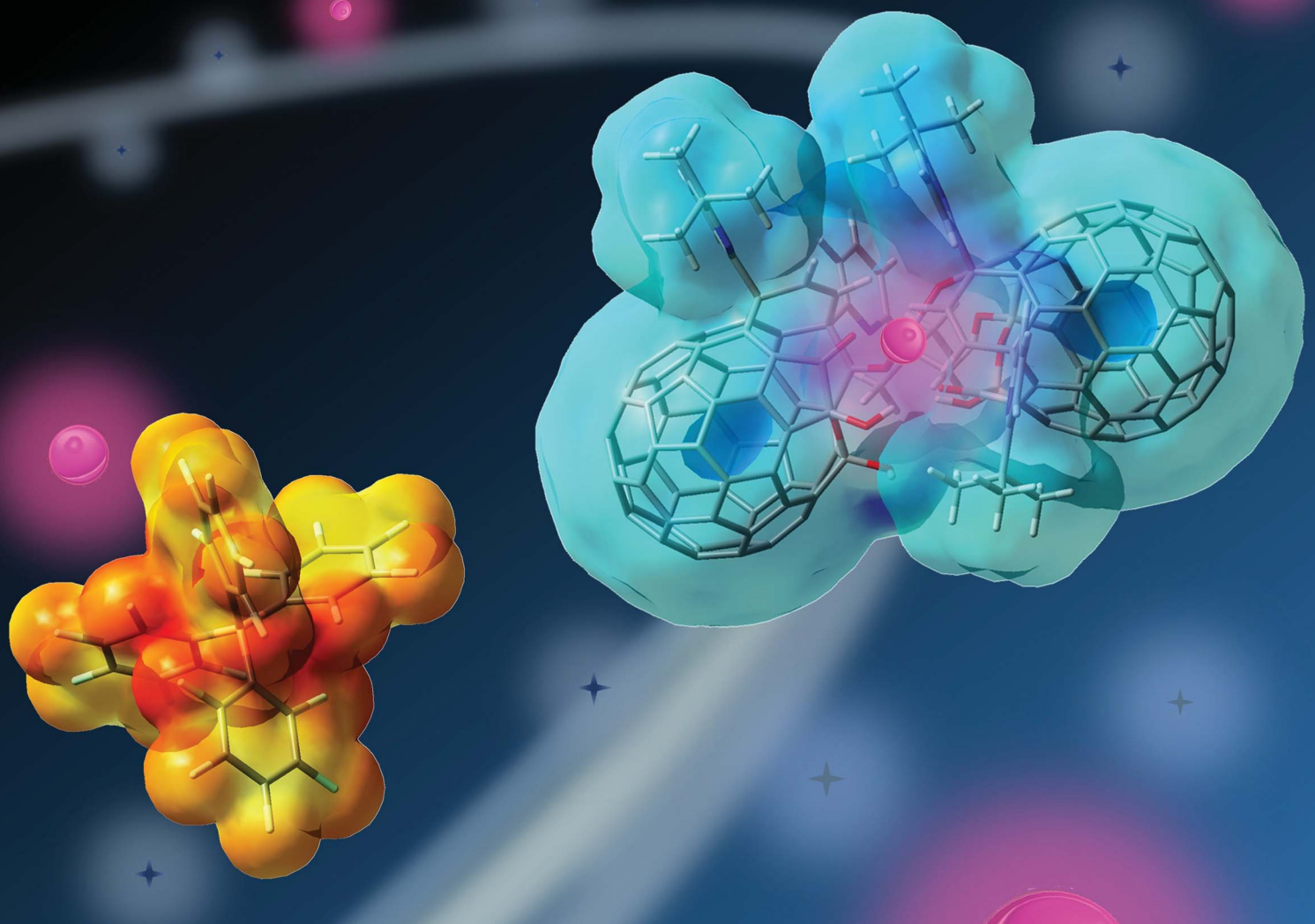


Chemical Science

rsc.li/chemical-science



ISSN 2041-6539



Cite this: *Chem. Sci.*, 2020, **11**, 12428

All publication charges for this article have been paid for by the Royal Society of Chemistry

Received 24th September 2020
 Accepted 16th October 2020

DOI: 10.1039/d0sc05280a
rsc.li/chemical-science

Introduction

Since the successful synthesis of cyclic polyethers by Pedersen in 1967,¹ a number of macrocyclic ligands have been produced in pursuit of their potential utilities in organic syntheses, metal sensors, ion carriers, and so forth.² Among macrocycles developed thus far, fully-conjugated planar systems are of particular importance to introduce additional features. Porphyrins and phthalocyanines are representative examples in which a variety of metal ions can be incorporated at the central rings, showing characteristic aromaticity and SMM (single-molecule magnet) properties.³ As curved ligands with spherical π -conjugation, truncated heterofullerenes were proposed by Karfunkel and coworkers in 1992.⁴ This hypothetical class of macrocycles can be described as pseudo-fullerenes in which two carbon atoms are at least removed from the C_{60} cage and heteroatoms are further replaced with the carbon atoms remaining on the thus-formed orifices. Currently, synthesis of truncated heterofullerenes still remains a formidable challenge while they potentially lead to the construction of spherical metal-organic frameworks as well as an isolation of a single metal atom or ion by passing through the macrocyclic orifice.⁵

In lieu of truncated heterofullerenes, open-cage C_{60} derivatives⁶ can be alternatively utilized for this purpose since they in

Cation recognition on a fullerene-based macrocycle[†]

Yoshifumi Hashikawa and Yasujiro Murata *

Heterocyclic orifices in cage-opened fullerene derivatives are regarded as potential ligands toward metals or ions, being reminiscent of truncated fullerenes as a hypothetical class of macrocycles with spherical π -conjugation. Among a number of cage-opened examples reported thus far, the coordination ability and dynamic behavior in solution still remained unclear due to difficulties in structural determination with multiple coordination sites on the macrocycles. Herein, we present the detailed solution dynamics of a cage-opened C_{60} derivative bearing a diketo bis(hemiketal) moiety in the presence of alkali metal ions. The NMR spectroscopy disclosed the coordination behavior which is identified as a two-step process with a 1 : 2 stoichiometry. Upon coordination to the Li^+ ion, the macrocycle largely varies its properties, *i.e.*, increased absorption coefficients in the visible region due to weakly-allowed charge transfer transitions as well as the inner potential field from neutral to positive by the charge delocalization along with the spherical π -surface. The Li^+ -complexes formed *in situ* underwent unprecedented selective dehydroxyhydrogenation under high-pressure conditions. These findings would facilitate further studies on fullerene-based macrocycles as metal sensors, bulky ligands in organic reactions, and ion carriers in batteries and biosystems.

general possess Lewis basic functional groups (Fig. 1). Nevertheless, the studies on fullerene-based macrocycles are quite limited⁷ because of the difficulty in structural characterization with multiple coordination sites on their rims of orifices, being in stark contrast to pristine C_{60} and its exohedral derivatives.^{8,9} In 2016, the first cage-opened C_{60} ligand toward $Cu^{(II)}$ was reported by Gan and co-workers.¹⁰ In 2018, they synthesized another types of ligand systems which coordinate with $Ni^{(II)}$,¹¹

Fullerene-based macrocyclic ligands:

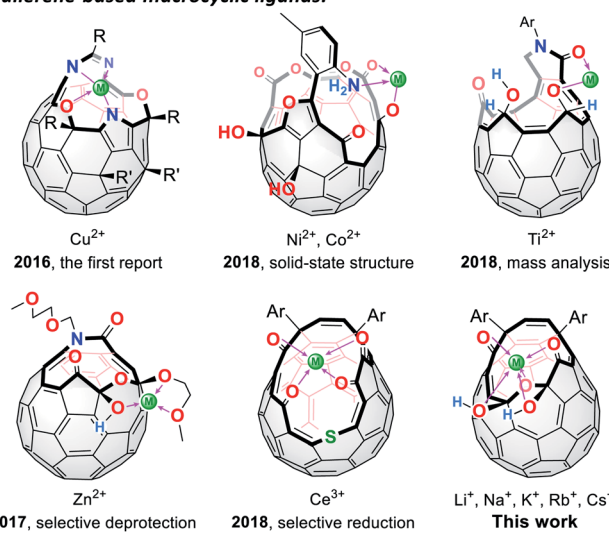


Fig. 1 Chemical structures of fullerene-based macrocyclic ligands.

Institute for Chemical Research, Kyoto University, Uji, Kyoto 611-0011, Japan. E-mail: yasujiro@scl.kyoto-u.ac.jp

† Electronic supplementary information (ESI) available: Detailed synthetic procedures, spectra, and optimized geometries. See DOI: [10.1039/d0sc05280a](https://doi.org/10.1039/d0sc05280a)



Co(II),¹¹ and Ti(II).¹² Around the same time, we also reported the Zn(II)¹³ and Ce(III)¹⁴ coordination on fullerene-based macrocycles, which resulted in selective deprotection and reduction, respectively. With these unique macrocycles exemplified above, however, the structures in solution accompanied by the association/dissociation dynamics have not yet been elucidated so far even though this is crucially informative for surveying properties of long-sought truncated heterofullerenes as well as for chemically synthesizing endohedral metallofullerenes. In this paper, we discuss the orifice flexibility on a cage-opened C₆₀ derivative having a diketo bis(hemiketal) moiety (Fig. 1), which enables coordination to alkali metal ions including Li⁺, Na⁺, K⁺, Rb⁺, and Cs⁺. By employing ⁷Li NMR titration, the coordination mode was examined in a solution, showing a 1 : 2 complexation with a Li⁺ ion. We also report the effect of the Li⁺-coordination on the rotational dynamics of the encapsulated H₂O molecule as well as the unprecedented Li^{+[B(C₆F₅)₄]⁻-mediated selective dehydroxyhydrogenation under high-pressure conditions.}

Results and discussion

A cage-opened C₆₀ ligand

We have previously reported the synthesis of **1** (Fig. 2a) as a precursor for the quantitative encapsulation of a water molecule inside its cage under high-pressure conditions.¹⁵ This compound has several coordination sites on its orifice, which are considered to work as ligands toward metals or ions. Different from common macrocyclic ligands in which unshared electron pairs involved in coordination are projected to the inner cavity, open-cage C₆₀ derivatives possess functional groups protruded unidirectionally, reflecting the orifice topology. In the case of diketo bis(hemiketal) **1**, the electrostatically negative potential field therefore emerges on its orifice as colored with red in Fig. 2b. Since the binding in complexes with alkali metal ions is in principle predominantly electrostatic,¹⁶ we examined the alkali-metal-ion affinity for **1** by NMR and absorption spectroscopies together with mass spectrometry.

Li⁺-coordination studied by NMR and absorption spectroscopies

Among alkali metals, lithium has an NMR active isotope with a natural abundance of 92.58% as ⁷Li ($I = 3/2$),¹⁷ which is

suitable for unveiling the solution dynamics of its complex with **1**. As a Li⁺-source, we selected lithium tetrakis(pentafluorophenyl)borate ethyl etherate (Li^{+[B(C₆F₅)₄]⁻·2.5Et₂O) showing a high solubility in common organic solvents. The NMR titration was conducted by adding a portion of **1** to a solution containing the lithium salt in *o*-dichlorobenzene-*d*₄ (ODCB-*d*₄). Fig. 3a represents the spectral change at the aromatic region in ¹H NMR. Upon increasing the ratio of Li⁺, the signals assignable to the pyridyl protons (shown as red and blue circles) became simple pairs of triplet and doublet ones, respectively, from a complicated signal pattern. This change was accompanied by the signal sharpening of ⁷Li with higher-field shift, getting closer to the free Li⁺ in ODCB-*d*₄ (Fig. 3b). These phenomena are suggestive of coordination/dissociation dynamics of the Li⁺ ion with **1**. To clarify where the Li⁺ ion locates, ¹³C NMR spectra were recorded using solutions of **1** with and without 20 equiv. of Li⁺ (Fig. 3c). Despite negligible change in aliphatic and aromatic regions, the lower field shifts}

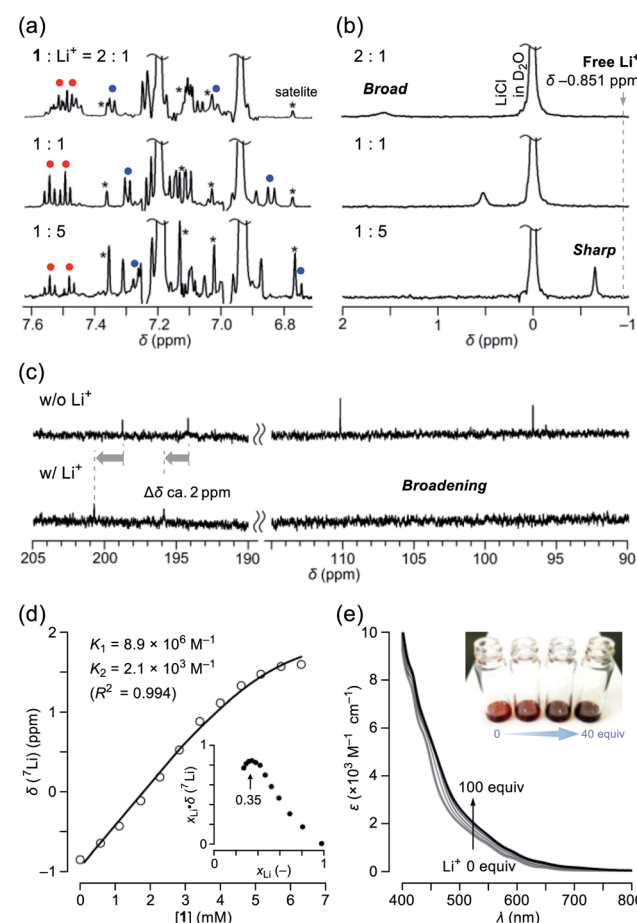


Fig. 3 Titration of Li^{+[B(C₆F₅)₄]⁻·2.5Et₂O by addition of **1** monitored by (a) ¹H NMR (500 MHz, ODCB-*d*₄, 300 K) and (b) ⁷Li NMR (194 MHz, ODCB-*d*₄, 300 K, LiCl/D₂O in a glass capillary as an external standard). (c) ¹³C NMR spectra of **1** without and with 20 equiv. of Li^{+[B(C₆F₅)₄]⁻·2.5Et₂O (126 MHz, ODCB-*d*₄). (d) Curve fitting data of the ⁷Li NMR chemical shifts. The inset shows the Job's plot. (e) Change in absorption spectra of **1** (1 mM in ODCB) by the addition of Li^{+[B(C₆F₅)₄]⁻·2.5Et₂O.}}}

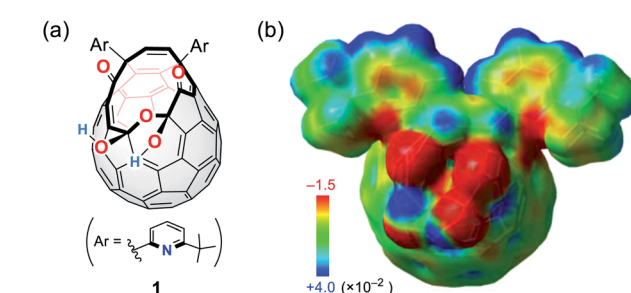


Fig. 2 (a) Structure of a cage-opened C₆₀ ligand **1** and (b) its electrostatic potential map around the orifice (MP2/6-31G(d,p)//M06-2X/6-31G(d,p)).



($\Delta\delta$ ca. +2 ppm) of the two carbonyl carbon signals were observed together with significant broadening of the two hemiketal carbon signals, presumably due to depleted electron densities caused by Li^+ -coordination and quadrupole effect of ^7Li , respectively. The Job's plot based on the ^7Li chemical shifts showed a maximum value at a mole fraction of 0.35, conclusively indicating the formation of a complex with a 1 : 2 stoichiometry, *i.e.*, $\text{Li}^+ \subset \mathbf{1}$ and $\text{Li}^+ \subset (\mathbf{1})_2$ (Fig. 3d). Since only a slight change in ^1H NMR spectra was observed at the Li^+ -content exceeding 1 equivalent (Fig. 3a), 1 : 2 complexation is considered to be less favored than 1 : 1 complexation ($K_1 > K_2$). By employing a 1 : 2 complexation model,¹⁸ we obtained association constants of $K_1 = 8.9 \times 10^6 \text{ M}^{-1}$ and $K_2 = 2.1 \times 10^3 \text{ M}^{-1}$, appearing negative cooperativity of $\alpha = K_1/4K_2 = 10^{-3} < 1$, while complexes $\text{Li}^+ \subset \mathbf{1}$ and $\text{Li}^+ \subset (\mathbf{1})_2$ were found to be considerably stable relative to $\text{Li}^+ + \mathbf{1}$ by $\Delta G = -9.5$ and $-4.6 \text{ kcal mol}^{-1}$, respectively. This bidding event caused significant change even in absorption spectra (Fig. 3e). Upon addition of Li^+ into the ODCB solution of $\mathbf{1}$, absorption coefficients in the visible region at 400–800 nm were obviously increased, concomitantly varying the solution color from reddish brown to dark black.

Alkali-metal-ion recognition

According to Pearson's HSAB (hard and soft acids and bases) principle,¹⁹ diketo bis(hemiketal) $\mathbf{1}$ possesses hard (OH groups) and soft (C=O groups) Lewis bases on its macrocyclic orifice. Hence, $\mathbf{1}$ is considered to have affinity toward a variety of metal ions from hard (Li^+) to soft (Cs^+) Lewis acids. Using a benzonitrile solution of $\mathbf{1}$ mixed with 1 equiv. of $\text{M}^+ \text{BPh}_4^-$ ($\text{M} = \text{Li, Na, K, Rb, and Cs}$), mass spectra were measured by applying the ESI (electrospray ionization) method. As confirmed by the NMR studies, a molecular ion peak of $\text{Li}^+ \subset \mathbf{1}$ was clearly observed at m/z 1127.2192 which is matched well with the calculated value (m/z 1127.2154) (Fig. 4a). Likewise, other alkali metal ions were also found to coordinate with $\mathbf{1}$. Notably, dimeric host-guest complexes $\text{M}^+ \subset (\mathbf{1})_2$ were suggested to be formed for all alkali metal ions despite lower magnitude of the peak intensities by a tenth compared with $\text{M}^+ \subset \mathbf{1}$ (Fig. 4b). In general, common macrocyclic ligands such as crown ethers and cryptands show the size-selectivity.²⁰ These results, however, indicate anomalous feature for $\mathbf{1}$ to capture alkali metal ions regardless of their ionic sizes even under mass spectrometric conditions at 200 °C, likely arising from a self-tunable coordination mode with a high degree of flexibility on the orifice. Conversely, the fact that the addition of alkali metal ions resulted in facile detection with high resolution also means that it would be helpful to characterize unstable and/or large molecular cage-opened C_{60} derivatives as we have previously observed.²¹

Theoretical models of coordination

To get insights into coordination modes of $\text{Li}^+ \subset \mathbf{1}$, theoretical calculations were performed at the M06-2X/6-31G(d,p) level of theory. Among three possible configurations, **C** was suggested to have the priority over **A** and **B** in terms of thermodynamic stability (Fig. 5, S8 and S15†). In the global minimum structure of **C**, the Li^+ ion locates on the center of the diketo

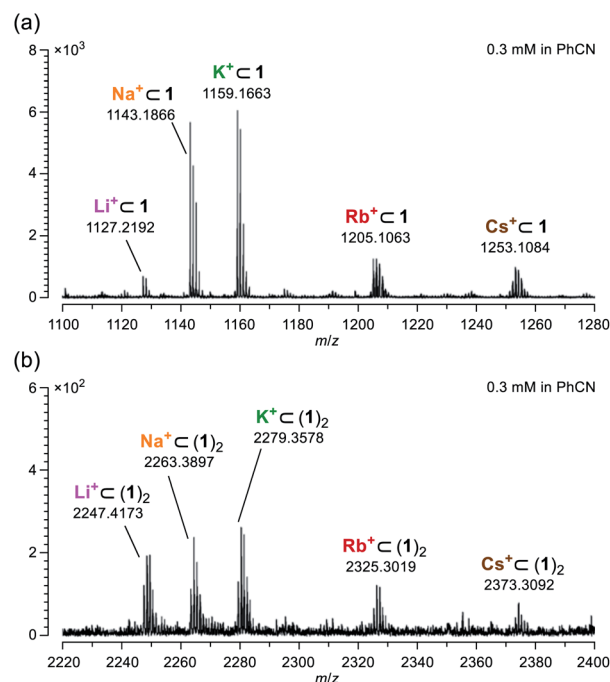


Fig. 4 Mass spectra of (a) $\text{M}^+ \subset \mathbf{1}$ and (b) $\text{M}^+ \subset (\mathbf{1})_2$ measured using a benzonitrile solution on ESI method.

bis(hemiketal) moiety which forms five dative bonds with distances of 1.89–2.34 Å, seemingly being the same as those in typical Li^+ -complexes (1.9–2.4 Å).¹⁶ This coordination mode is in excellent accordance with the structure determined experimentally as described above. The similar configurations were suggested for $\text{M}^+ \subset \mathbf{1}$ by the calculations at the M06-2X level of

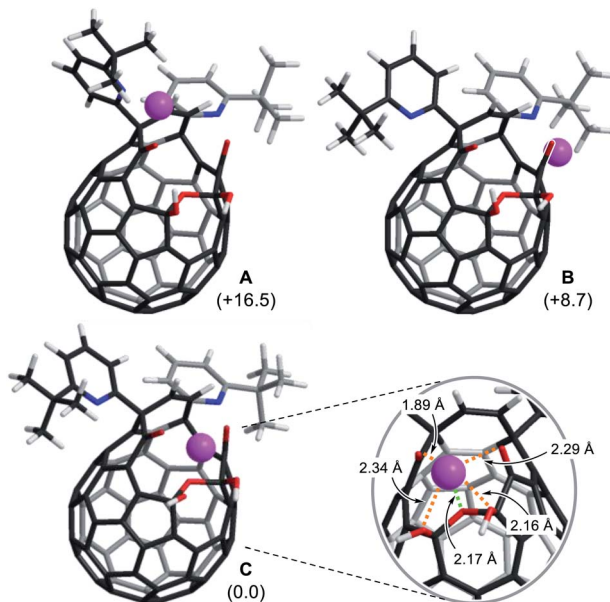


Fig. 5 Three possible coordination modes of $\mathbf{1}$ toward Li^+ (M06-2X/6-31G(d,p)). The values in parentheses represent the differences in Gibbs energies at 298 K.



theory with the basis sets of LanL2DZ for alkali metals and 6-31G(d,p) for the rest. As listed in Table 1, all alkali metal ions would form thermodynamically stable complexes $M^+ \subset \mathbf{1}$ in which the stabilization energies decrease with increasing atomic number whereas the distances between oxygen atoms (*a*–*d*) on **1** get longer in a concentric fashion, further supporting a great flexibility of the fullerene-based macrocyclic ligand. Considering the changes in Gibbs energies, **1** could be regarded as a hard Lewis basic ligand rather than soft one.

To get more details on the observed absorption behavior of **1** in the presence of Li^+ , TD DFT calculations were conducted at the CAM-B3LYP/6-31G(d)//B3LYP/6-31G(d) level of theory. The Li^+ -coordination on **1** causes lowering of the LUMO level from –3.13 to –3.74 eV as well as a considerable drop of energy levels of the HOMO (–5.80 eV) and HOMO–1 (–5.83 eV) for **1** into those of the HOMO–3 (–6.40 eV) and HOMO–4 (–6.43 eV) for $(\text{Li}^+ \subset \mathbf{1})[\text{B}(\text{C}_6\text{F}_5)_4]^-$ in which the HOMO and HOMO–1 are now localized on a part of the counter anion (Fig. S14†). The oscillator strengths at optical transitions over 400 nm were plotted in Fig. 6a and b. Whereas the two plots of **1** and $(\text{Li}^+ \subset \mathbf{1})[\text{B}(\text{C}_6\text{F}_5)_4]^-$ showed close resemblance with each other, the number of weakly-allowed transitions are definitely increased (34 to 49), rationally explaining the intense solution color of **1** by the addition of Li^+ . Upon seeing the two of newly-appeared transitions at the longest wavelengths of $\lambda = 531$ and 519 nm (marked with a circle in Fig. 6b), these absorption bands in the visible region are attributed to intra- and intermolecular charge transfer (CT) transitions corresponding to the HOMO–2 \rightarrow LUMO+3 (contribution: 27%) and HOMO–5 \rightarrow LUMO+2 (15%) with a oscillator strength of $f = 0.0066$ ($\lambda = 531$) as well as the HOMO–3 \rightarrow LUMO+3 (30%) and HOMO–2 \rightarrow LUMO+3 (18%) with $f = 0.0065$ ($\lambda = 519$) (Fig. 6c). To verify the role of the counter anion, we also calculated the transition energies for $\text{Li}^+ \subset \mathbf{1}$, showing the increased number of weakly-allowed transitions, relative to **1** (34 to 42), with an intramolecular CT character such as the HOMO–1 \rightarrow LUMO+2 transition (27%) with $f = 0.013$ at $\lambda = 555$ nm (Fig. S13†). The observed intense

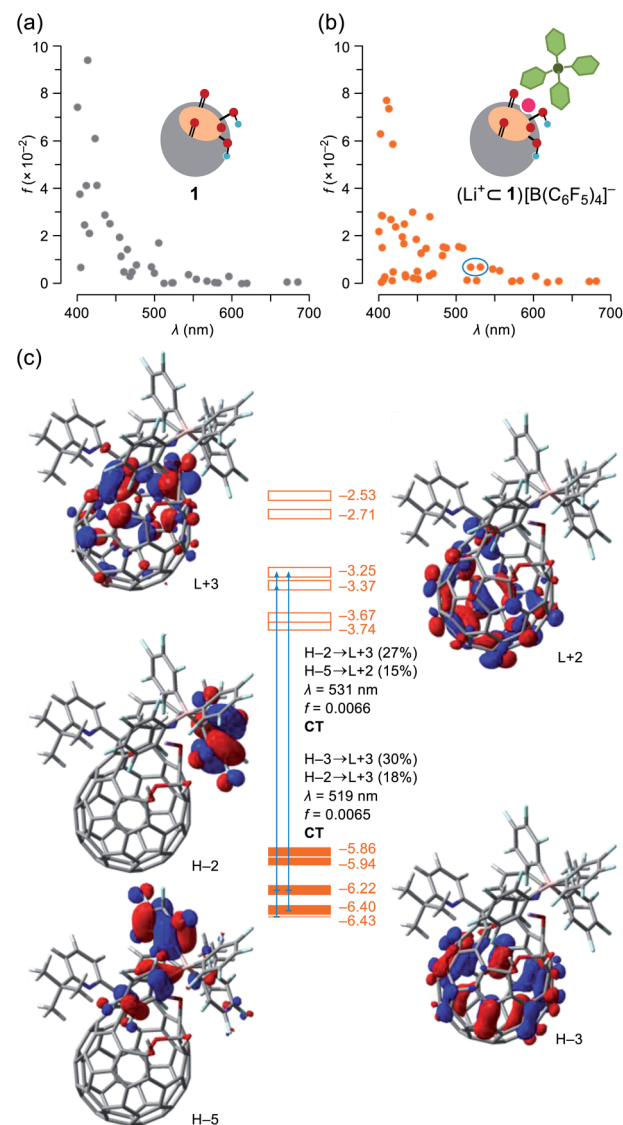


Fig. 6 Plots of oscillator strengths for (a) **1** and (b) $(\text{Li}^+ \subset \mathbf{1})[\text{B}(\text{C}_6\text{F}_5)_4]^-$ with (c) pictorial representation of the HOMOs and LUMOs, abbreviated as H and L, respectively. The transition energies were calibrated with a factor of 0.72²² (TD-CAM-B3LYP/6-31G(d)//B3LYP/6-31G(d)).

Table 1 Complexation of **1** with alkali metal ions^a

M^+	ΔG (kcal mol ^{–1})	$M^+ \subset \mathbf{1}$			
		<i>a</i> (Å)	<i>b</i> (Å)	<i>c</i> (Å)	<i>d</i> (Å)
Li^+	–53.2	3.14	3.70	3.13	3.17
K^+	–30.0	3.26	3.77	3.16	3.40
Na^+	–17.3	3.34	3.81	3.18	3.56
Rb^+	–9.2	3.37	3.83	3.18	3.65
Cs^+	–4.1	3.36	3.84	3.17	3.69

^a Calculated at the M06-2X level of theory with basis sets of LanL2DZ for alkali metal ions and 6-31G(d,p) for the rest.

absorption in **1** upon addition of Li^+ is therefore triggered by the Li^+ -coordination which promotes intra- and intermolecular CT transitions with larger oscillator strengths compared with pristine **1**.

Effect of Li^+ -coordination on rotational dynamics of entrapped H_2O molecules

To probe the physical picture inside **1**, the incarcerated H_2O molecule could be utilized as a magnetic measure in NMR which tells the rotational dynamics inside the spherical electrostatic potential field.²³ According to the reported method, $\text{H}_2\text{O}@\mathbf{1}$ was prepared.¹⁵ Curiously enough, the high-field region in the NMR spectrum of $\text{H}_2\text{O}@\mathbf{1}$ with $\text{Li}^+[\text{B}(\text{C}_6\text{F}_5)_3]^- \cdot 2.5\text{Et}_2\text{O}$ exhibited three singlet signals at δ –9.98, –10.13, and –10.23 ppm, indicative of the H_2O molecules existing in



different chemical environment (Fig. 7a). The two signals at δ –9.98 and –10.13 ppm were observed only in the presence of the lithium salt whereas their signal intensities diminished substantially at the elevated temperature. The PFG (pulsed field-gradient) NMR spectroscopy²⁴ revealed the different diffusion coefficients D and effective hydrodynamic radii r_H for these three chemical species assignable to $\text{H}_2\text{O}@\mathbf{1}$ (δ –10.23 ppm), $\text{Li}^+ \subset (\text{H}_2\text{O}@\mathbf{1})$ (δ –10.13 ppm), and $\text{Li}^+ \subset (\text{H}_2\text{O}@\mathbf{1})_2$ (δ –9.98 ppm) whilst the molecular size of the last one was underestimated presumably due to the deviation from the hypothetical Brownian motion, caused by its dimeric structure largely different from a shape of a particle.

Importantly, full widths at half maximum of the ^1H signals were found to be increased by the Li^+ -coordination, implying the change in relaxation mechanism or dynamic behavior (Fig. 7a). Thus, the longitudinal and transverse relaxation times (T_1 and T_2) were measured in degassed ODCB- d_4 within a temperature range of 290–330 K under a field strength of 800 MHz. As depicted in Fig. 7b, the T_1 values were increased by lowering the temperature, demonstrative of the dominant relaxation *via* spin-rotation mechanism,²⁵ irrespective of the existence of Li^+ . This indicates that the distance between $(^1\text{H})_2\text{O}$ and $^7\text{Li}^+$ is far enough to interact magnetically each other. The shortened T_2 values by the Li^+ -coordination are consistent with the observed signal broadening. The large T_1 – T_2 gaps in $\text{Li}^+ \subset (\text{H}_2\text{O}@\mathbf{1})_n$ ($n = 1, 2$) indicate the restricted motion of the H_2O molecules.^{14,26} Upon assuming the spin-rotation mechanism as the sole contribution to the ^1H relaxation,²⁷ angular momentum correlation times τ_J (330 K) were obtained to be less than 1 ps, showing close resemblance to the dynamic behavior of supercritical water.²⁸ Considering the Arrhenius-type thermal activation process,²⁹ the rotational barriers of the H_2O

molecules were experimentally determined to be 0.88 ± 0.13 for $\text{H}_2\text{O}@\mathbf{1}$, 1.44 ± 0.03 for $\text{Li}^+ \subset (\text{H}_2\text{O}@\mathbf{1})$, and 1.41 ± 0.09 kcal mol^{–1} for $\text{Li}^+ \subset (\text{H}_2\text{O}@\mathbf{1})_2$, respectively (Fig. 3c).

Since the dynamic behavior of water inside hydrophobic subnanospace is explainable by the different interaction strength between water and the wall,³⁰ electrostatic potential fields inside $\mathbf{1}$ and $(\text{Li}^+ \subset \mathbf{1})[\text{B}(\text{C}_6\text{F}_5)_4]^-$ were computed at the MP2/6-31G(d,p)//M06-2X/6-31G(d,p) level of theory. As drawn in Fig. 8a, the inner potential surface of $\mathbf{1}$ seems to be neutral. A partial negative charge nearby the orifice has negligible perturbation toward the rotational motion of H_2O since the H-bonded conformation (O···O distance: 3.33 Å)^{14,31} is suggested to be thermodynamically unfavorable by $\Delta G +1.07$ kcal mol^{–1} relative to non-bonded one (3.77 Å) (Fig. 8 and S10†). The Li^+ -coordination causes a significant change in the potential field: delocalization of the cationic charge both inside and outside the π -framework, rendering the water orientation at the center of the cage to maximize enthalpy gain *via* the electrostatic interaction. Considering the stabilization energies ΔG_{water} given by the H_2O -encapsulation, $(\text{Li}^+ \subset \mathbf{1})[\text{B}(\text{C}_6\text{F}_5)_4]^-$ has a larger energetic gain by $\Delta \Delta G_{\text{water}}$ 0.77 kcal mol^{–1} compared with $\mathbf{1}$. This is comparable to the observed difference in rotational barriers (ΔE_a 0.56 kcal mol^{–1}). Thus, the rotational motion of the H_2O molecules in $\mathbf{1}$ and $\text{Li}^+ \subset \mathbf{1}$ is regarded to be governed by the van der Waals and electrostatic interactions, respectively.

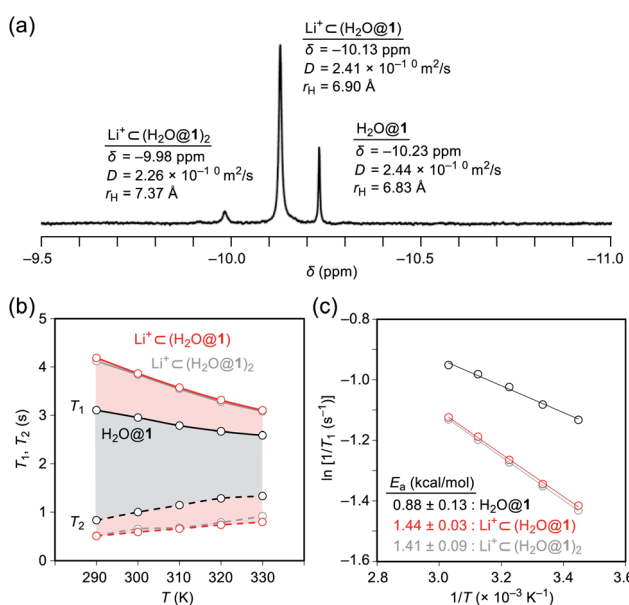


Fig. 7 (a) ^1H NMR spectrum (500 MHz, ODCB- d_4), (b) temperature dependence of relaxation times (errors less than 5%), and (c) Arrhenius plots ($\ln 1/T_1$ vs. $1/T$) of $\text{H}_2\text{O}@\mathbf{1}$ with 20 equiv. of $\text{Li}^+[\text{B}(\text{C}_6\text{F}_5)_3]^- \cdot 2.5\text{Et}_2\text{O}$ (800 MHz, ODCB- d_4).

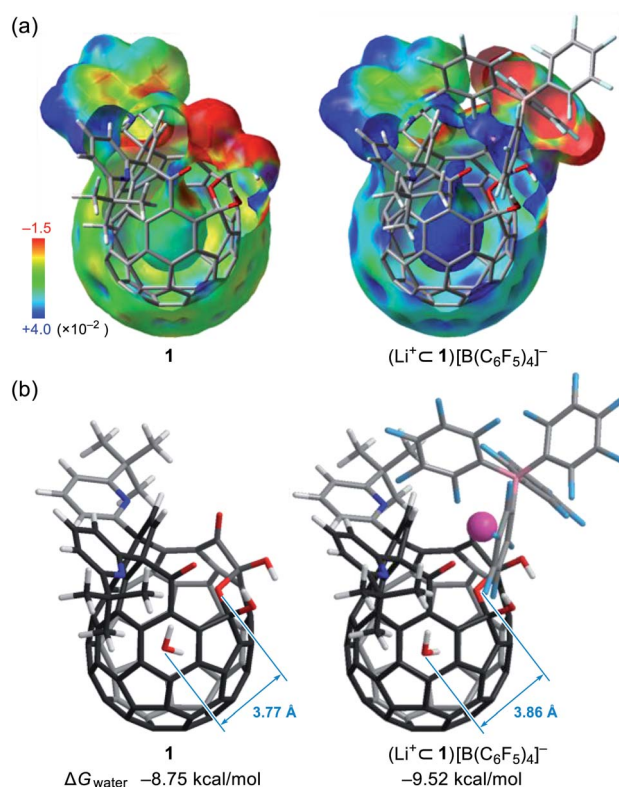


Fig. 8 (a) Electrostatic potential maps inside $\mathbf{1}$ and $(\text{Li}^+ \subset \mathbf{1})[\text{B}(\text{C}_6\text{F}_5)_4]^-$ (MP2/6-31G(d,p)//M06-2X/6-31G(d,p)). (b) Global minimum structures of $\text{H}_2\text{O}@\mathbf{1}$ and $(\text{Li}^+ \subset \text{H}_2\text{O}@\mathbf{1})[\text{B}(\text{C}_6\text{F}_5)_4]^-$ (M06-2X/6-31G(d,p), 298 K).



$\text{Li}^+[\text{B}(\text{C}_6\text{F}_5)_4]^-$ -mediated dehydroxyhydrogenation under high pressure

Subsequently, we turned our focus to high-pressure effect on the complexation of **1** with Li^+ . Initially, we expected either precipitation of $(\text{Li}^+ \subset (\mathbf{1})_2)[\text{B}(\text{C}_6\text{F}_5)_4]^-$ by lowering its solubility under high pressure conditions or formation of $(\text{Li}^+ @ \mathbf{1})[\text{B}(\text{C}_6\text{F}_5)_4]^-$ as stable salts. Hence, the solution of **1** and $\text{Li}^+[\text{B}(\text{C}_6\text{F}_5)_4]^- \cdot 2.5\text{Et}_2\text{O}$ in ODCB was subjected to a pressure of 10 000 atm at 130 °C for 24 h (Table 2). After the treatment, the crude mixture still maintained homogeneity without precipitation, suggestive of negligible pressure effect on the solubility of the lithium salt sandwiched with two cage-opened C_{60} ligands. The ^7Li NMR measurement of the crude mixture confirmed no encapsulation of a Li^+ ion inside **1**. Theoretical calculations suggested that the Li^+ -encapsulation is thermodynamically unfavored ($\Delta G = +26.0 \text{ kcal mol}^{-1}$). Instead, we found the formation of $\text{H}_2\text{O} @ \mathbf{3}$ in which one of the hydroxy groups in **1** was replaced with a hydrogen atom.^{13,32} Under these conditions, a water molecule released from the bis(hemiketal) moiety of **1** was trapped inside the cavity of **2** which was formed *in situ*,^{15,33} thus affording $\text{H}_2\text{O} @ \mathbf{1}$ and $\text{H}_2\text{O} @ \mathbf{3}$ after chromatographic purification. Importantly, $\text{H}_2\text{O} @ \mathbf{3}$ was not formed in the absence of $\text{Li}^+[\text{B}(\text{C}_6\text{F}_5)_4]^-$ (entry 1). By employing 0.2 equiv. of $\text{Li}^+[\text{B}(\text{C}_6\text{F}_5)_4]^-$, $\text{H}_2\text{O} @ \mathbf{3}$ was obtained in 6% isolated yield with an occupation level of H_2O being 96%. This indicates that the conversion of **1** into **3** is kinetically less preferred relative to the insertion of H_2O into **2**. By increasing the amount of $\text{Li}^+[\text{B}(\text{C}_6\text{F}_5)_4]^-$, the yield of $\text{H}_2\text{O} @ \mathbf{3}$ was improved up to 34% with a significantly decreased occupation level of H_2O from 96 to 75% probably due to (i) the formation of lithium hydrates $\text{Li}^+(\text{H}_2\text{O})_n$, (ii) prevented dehydration from **1** by the Li^+ -coordination onto **1**, or (iii) prevented H_2O -insertion by the Li^+ -coordination onto **2** (entries 2–4). Contrastingly, the addition of the excessive amount of water resulted in lowering yield of $\text{H}_2\text{O} @ \mathbf{3}$ (17%) with an elevated occupation level of H_2O (88%) (entry 5). It should be noted that this reaction did not proceed well under ambient pressure (entry 6).

Table 2 $\text{Li}^+[\text{B}(\text{C}_6\text{F}_5)_4]^-$ -mediated dehydroxyhydrogenation of **1**

Entry	$\text{Li}^+[\text{B}(\text{C}_6\text{F}_5)_4]^-$	H_2O	$\text{H}_2\text{O} @ \mathbf{3}^a$
1	—	Excess	Not formed
2	0.2 equiv.	—	6% (96%)
3	1.0 equiv.	—	23% (94%)
4	10 equiv.	—	34% (75%)
5	10 equiv.	Excess	17% (88%)
6 ^b	10 equiv.	—	Trace

^a Isolated yields. Values in parentheses are encapsulation ratio of H_2O determined by ^1H NMR. ^b Conducted under ambient pressure.

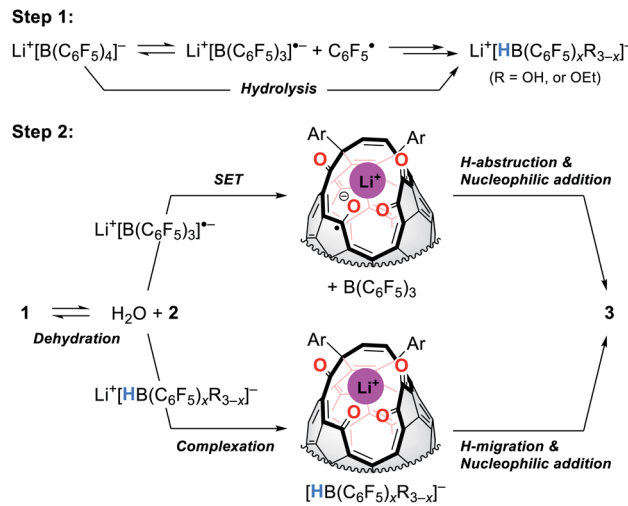


Fig. 9 Plausible mechanism.

Fig. 9 shows the proposed mechanism consisting of two steps. Under high-pressure conditions, this reaction is considered to be initiated with the homolytic cleavage of the C–B bond in $\text{Li}^+[\text{B}(\text{C}_6\text{F}_5)_4]^-$,³⁴ giving a radical anion of triarylborane, *i.e.*, $\text{B}(\text{C}_6\text{F}_5)_3\cdot^-$ which is a stable organic radical species owing to its structure isoelectronic to triarylmethyl radicals.³⁵ In solution, however, $\text{B}(\text{C}_6\text{F}_5)_3\cdot^-$ is known to decompose to furnish four-coordinate borate species bearing a B–H bond such as $\text{HB}(\text{C}_6\text{F}_5)_3^-$ *via* solvolytic radical reactions.³⁶ The similar borate species could be generated from $\text{Li}^+[\text{B}(\text{C}_6\text{F}_5)_4]^-$ which is transformed into $\text{B}(\text{C}_6\text{F}_5)_x\text{R}_{3-x}$ *via* aryl migration followed by hydrolysis.³⁷ The further hydride abstraction from solvents provides $[\text{HB}(\text{C}_6\text{F}_5)_x\text{R}_{3-x}]^-$.³⁸ The mass spectrometric analysis of the crude mixture showed molecular ion peaks possibly assignable to $\text{B}(\text{C}_6\text{F}_5)_3$, $\text{B}(\text{C}_6\text{F}_5)_2\text{OH}$, and $\text{B}(\text{C}_6\text{F}_5)_2\text{OEt}$, supporting the partial decomposition of $\text{Li}^+[\text{B}(\text{C}_6\text{F}_5)_4]^-$. In the second step, **1** will lose a water molecule from its orifice to afford **2**. During this equilibrium, the water molecule is encapsulated inside **2** which works as a desiccant to prevent the decomposition of active borane and borate species generated in the first step. Tetraketo derivative **2** then undergoes single-electron transfer (SET) to provide a ketyl radical complex ($\text{Li}^+ \subset 2\cdot^-$) which is eventually converted into **3** *via* H-abstraction with an intramolecular nucleophilic addition. Another possible route is commenced with the complexation of $\text{Li}^+[\text{HB}(\text{C}_6\text{F}_5)_x\text{R}_{3-x}]^-$ on **2**, followed by H-migration with an $\text{S}_{\text{N}}2'$ -type cyclization. In both these two pathways, Li^+ -coordination would facilitate the bond polarization of the carbonyl group. This reaction is, as a consequence, accompanied by the formation/regeneration of three-coordinate boron compounds, *i.e.*, $\text{B}(\text{C}_6\text{F}_5)_3$ or $\text{B}(\text{C}_6\text{F}_5)_x\text{R}_{3-x}$, as observed experimentally.

Conclusions

In summary, we disclosed the solution dynamics of a fullerene-based macrocyclic ligand **1** in the presence of a Li^+ ion. The NMR spectroscopy demonstrated the coordination of the Li^+ ion to the diketo bis(hemiketal) moiety in **1** with 1 : 1 and 1 : 2



stoichiometries which were identified with the association constants of $K_1 = 8.9 \times 10^6 \text{ M}^{-1}$ ($\text{Li}^+ \subset \mathbf{1}$) and $K_2 = 2.1 \times 10^3 \text{ M}^{-1}$ ($\text{Li}^+ \subset (\mathbf{1})_2$). The mass spectrometric analyses further suggested the formation of the 1 : 2 complexes even for other alkali metal ions including Na^+ , K^+ , Rb^+ , and Cs^+ , indicative of the flexibility of **1** as the Lewis basic ligand. Upon complexation of **1** with Li^+ , intense absorption was induced in the visible region by intra- and intermolecular CT transitions. Intriguingly, the Li^+ -coordination caused major perturbations to the electrostatic potential field inside **1** from neutral to positive, which was confirmed by the use of incarcerated H_2O molecules as magnetic probes, demonstrating the considerable restriction on its rotational dynamics particularly at lower temperatures accompanied by the increase of the T_1 values. By exposure to high-pressure conditions, complexes $\text{Li}^+ \subset (\mathbf{1})_n$ ($n = 1, 2$) that formed *in situ* underwent unprecedented dehydroxyhydrogenation to furnish **3** in a moderate yield. This reaction occurred only under high pressure conditions in the presence of $\text{Li}^+[\text{B}(\text{C}_6\text{F}_5)_4]^-$, in which $\text{B}(\text{C}_6\text{F}_5)_3 \cdot^-$ and $[\text{HB}(\text{C}_6\text{F}_5)_x\text{R}_{3-x}]^-$ would be actual active species. The characteristic association behavior and reactivity of the fullerene-based macrocycles would potentially provide utilities as metal sensors with tunable electronic configurations, batteries with modifiable ionic conductivities, and polydentate bulky ligands in organic reactions, as well as a guidepost for the long-awaited chemical synthesis of metallofullerenes.

Conflicts of interest

There are no conflicts to declare.

Acknowledgements

Financial support was partially provided by the JSPS KAKENHI Grant Number JP17H06119, JP20K15260, and JP20H05218. The NMR measurements were partly supported by the Joint Usage/Research Center (JURC) at the ICR, Kyoto University.

Notes and references

- 1 C. J. Pedersen, *J. Am. Chem. Soc.*, 1967, **89**, 7017–7036.
- 2 (a) G. W. Gokel, W. M. Leevy and M. E. Weber, *Chem. Rev.*, 2004, **104**, 2723–2750; (b) Z. Liu, S. K. M. Nalluri and J. F. Stoddart, *Chem. Soc. Rev.*, 2017, **46**, 2459–2478.
- 3 (a) S. Saito and A. Osuka, *Angew. Chem., Int. Ed.*, 2011, **50**, 4342–4373; (b) H. Lu and N. Kobayashi, *Chem. Rev.*, 2016, **116**, 6184–6261; (c) E. A. Kuzmina, T. V. Dubinina and L. G. Tomilova, *New J. Chem.*, 2019, **43**, 9314–9327.
- 4 H. R. Karfunkel, T. Dressler and A. Hirsch, *J. Comput.-Aided Mol. Des.*, 1992, **6**, 521–535.
- 5 A. Hirsch, *Fullerenes: Chemistry and Reactions*, Wiley-VCH Verlag GmbH & Co. KGaA, Weinheim, 2005.
- 6 (a) Y. Rubin, *Chem.-Eur. J.*, 1997, **3**, 1009–1016; (b) M. Murata, Y. Murata and K. Komatsu, *Chem. Commun.*, 2008, 6083–6094; (c) G. C. Vougioukala-Kis, M. M. Roubelakis and M. Orfanopoulos, *Chem. Soc. Rev.*, 2010, **39**, 817–844; (d) L. Shi and L. Gan, *J. Phys. Org. Chem.*, 2013, **26**, 766–772.
- 7 Y. Li and L. Gan, *Chem.-Eur. J.*, 2017, **23**, 10485–10490.
- 8 (a) P. J. Fagan, J. C. Calabrese and B. Malone, *Acc. Chem. Res.*, 1992, **25**, 134–142; (b) A. L. Balch and M. M. Olmstead, *Chem. Rev.*, 1998, **98**, 2123–2165; (c) W.-Y. Yeh, *J. Organomet. Chem.*, 2015, **784**, 13–23.
- 9 (a) Y. Hashikawa, M. Murata, A. Wakamiya and Y. Murata, *Org. Lett.*, 2016, **18**, 6348–6351; (b) H. Zhang, Z. Zhou, L. Yang, J. Su, P. Jin and L. Gan, *Organometallics*, 2019, **38**, 3139–3143.
- 10 Y. Li, G. Zhang, D. Wang, B. Xu, D. Xu, N. Lou and L. Gan, *Angew. Chem., Int. Ed.*, 2016, **55**, 14590–14594.
- 11 Z. Zhou, N. Xin and L. Gan, *Chem.-Eur. J.*, 2018, **24**, 451–457.
- 12 H. Zhang, C. Pan, X. Lu and L. Gan, *Org. Chem. Front.*, 2019, **6**, 1397–1402.
- 13 Y. Hashikawa, M. Murata, A. Wakamiya and Y. Murata, *Can. J. Chem.*, 2017, **95**, 320–328.
- 14 Y. Hashikawa, S. Hasegawa and Y. Murata, *Chem. Commun.*, 2018, **54**, 13686–13689.
- 15 K. Kurotobi and Y. Murata, *Science*, 2011, **33**, 613–616.
- 16 U. Olsher, *Chem. Rev.*, 1991, **91**, 137–164.
- 17 H. Günther, Lithium NMR, in *Encyclopedia of Magnetic Resonance*, John Wiley & Sons, Ltd, Chichester, UK, 2007.
- 18 P. Thordarson, *Chem. Soc. Rev.*, 2011, **40**, 1305–1323.
- 19 R. G. Pearson, *J. Am. Chem. Soc.*, 1963, **85**, 3533–3539.
- 20 J. J. Christensen, D. J. Eatough and R. M. Izatt, *Chem. Rev.*, 1974, **74**, 351–384.
- 21 Y. Hashikawa and Y. Murata, *Chem.-Eur. J.*, 2019, **25**, 2482–2485.
- 22 (a) Y. Hashikawa, H. Yasui, K. Kurotobi and Y. Murata, *Mater. Chem. Front.*, 2018, **2**, 206–213; (b) Y. Hashikawa, S. Okamoto and Y. Murata, *Commun. Chem.*, 2020, **3**, 90.
- 23 Y. Li, J. Y.-C. Chen, X. Lei, R. G. Lawler, Y. Murata, K. Komatsu and N. J. Turro, *J. Phys. Chem. Lett.*, 2012, **3**, 1165–1168.
- 24 Y. Cohen, L. Avram and L. Frish, *Angew. Chem., Int. Ed.*, 2005, **44**, 520–554.
- 25 E. Sartori, M. Ruzzi, N. J. Turro, J. D. Decatur, D. C. Doetschman, R. G. Lawler, A. L. Buchachenko, Y. Murata and K. Komatsu, *J. Am. Chem. Soc.*, 2006, **128**, 14752–14753.
- 26 Y. Hashikawa, M. Murata, A. Wakamiya and Y. Murata, *J. Am. Chem. Soc.*, 2016, **138**, 4096–4104.
- 27 P. S. Hubbard, *Phys. Rev.*, 1963, **131**, 1155–1165.
- 28 W. J. Lamb and J. Jonas, *J. Chem. Phys.*, 1981, **74**, 913–921.
- 29 (a) J. Jonas, T. DeFries and W. J. Lamb, *J. Chem. Phys.*, 1978, **68**, 2988–2989; (b) Y. Hashikawa and Y. Murata, *J. Am. Chem. Soc.*, 2019, **141**, 12928–12938; (c) Y. Hashikawa and Y. Murata, *Chem. Lett.*, 2020, **49**, 244–247.
- 30 (a) H. Kyakuno, K. Matsuda, Y. Nakai, R. Ichimura, T. Saito, Y. Miyata, K. Hata and Y. Maniwa, *Sci. Rep.*, 2017, **7**, 14834; (b) Y. Hashikawa, M. Murata, A. Wakamiya and Y. Murata, *Angew. Chem., Int. Ed.*, 2016, **55**, 13109–13113; (c) Y. Hashikawa and Y. Murata, *J. Am. Chem. Soc.*, 2017, **139**, 18468–18471.
- 31 M. D. Battistel, H. F. Azurmendi, M. Frank and D. I. Freedberg, *J. Am. Chem. Soc.*, 2015, **137**, 13444–13447.



32 A. Krachmalnicoff, M. H. Levitt and R. J. Whitby, *Chem. Commun.*, 2014, **50**, 13037–13040.

33 Y. Hashikawa, M. Murata, A. Wakamiya and Y. Murata, *Org. Lett.*, 2014, **16**, 2970–2973.

34 (a) T. Onak, *Organoborane Chemistry*, Academic Press, Inc., New York, 1975; (b) S. N. Mlondo, P. O'Brien, P. J. Thomas, M. Hellwell, J. Raftery and D. J. Procter, *Chem. Commun.*, 2008, 2456–2458.

35 T. Kushida and S. Yamaguchi, *Organometallics*, 2013, **32**, 6654–6657.

36 E. J. Lawrence, V. S. Oganesyan, G. G. Wildgoose and A. E. Ashley, *Dalton Trans.*, 2013, **42**, 782–789.

37 P. J. Grisdale, J. L. R. Williams, M. E. Glogowski and B. E. Babb, *J. Org. Chem.*, 1971, **36**, 544–549.

38 M. Shang, J. Z. Chan, M. Cao, Y. Chang, Q. Wang, B. Cook, S. Torker and M. Wasa, *J. Am. Chem. Soc.*, 2018, **140**, 10593–10601.

